analytical chemistry

Article

pubs.acs.org/ac

Standoff Mechanical Resonance Spectroscopy Based on Infrared-Sensitive Hydrogel Microcantilevers

Inseok Chae,[†] M. Faheem Khan,[†] Jungki Song,[‡] Taewook Kang,[§] Jungchul Lee,*[,‡] and Thomas Thundat*[,†]

[†]Department of Chemical and Materials Engineering, University of Alberta, Edmonton, Alberta T6G 2V4, Canada

[‡]Department of Mechanical Engineering, and [§]Department of Chemical and Biomolecular Engineering, Sogang University, Seoul 04107, South Korea

Supporting Information

ABSTRACT: This paper reports a highly sensitive and selective remote chemical sensing platform for surface-adsorbed trace chemicals by using infrared (IR)-sensitive hydrogel microcantilevers. Poly(ethylene glycol) diacrylate (PEG-DA) hydrogel microcantilevers are fabricated by ultraviolet (UV) curing of PEG-DA prepolymer introduced into a poly(dimethylsiloxane) mold. The resonance frequency of a PEG-DA microcantilever exhibits high thermal sensitivity due to IR irradiation/absorption. When a tunable IR laser beam is reflected off a surface coated with target chemical onto a PEG-DA microcantilever, the resonance frequency of the cantilever shifts in proportion to the chemical nature of the target molecules. Dynamic responses of the PEG-DA microcantilever can be obtained in a range of IR wavelengths using a tunable quantum cascade laser that can form the basis for the standoff mechanical resonance spectroscopy (SMRS). Using this SMRS technique, we have selectively detected three compounds, dimethyl methyl phosphonate (DMMP), cyclotrimethylene trinitramine (RDX), and pentaerythritol tetranitrate (PETN), located 4 m away from the PEG-DA microcantilever detector. The experimentally measured limit of detection for PETN trace using the PEG-DA microcantilever was 40 ng/cm^2. Overall, the PEG-DA microcantilever is a promising candidate for further exploration and optimization of standoff detection methods.

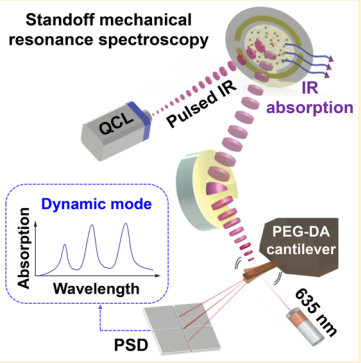

There have been many ongoing efforts to develop techniques that can detect hazardous materials sensitively and selectively while providing a maximum safety to field operators. Standoff spectroscopy is one of the safest detection techniques which can chemically recognize remotely placed target analytes with high sensitivity and selectivity.[1−3] It has been mainly employed for the detection of hazardous materials such as explosives, flammable agents, and biological threats since operators stay at a safe distance away from the suspected targets.[4−6] This remote sensing capability as well as high selectivity make the standoff spectroscopic techniques well-suited for dangerous materials detection and/or monitoring.[7] Standoff spectroscopies based on Raman, infrared (IR), and laser-induced breakdown generally employ a laser to exploit coherence and small divergence which are preferred for remote detection with high selectivity[8−11] along with an optical detector. In such laser-based standoff techniques, a laser beam strikes a target surface at a distance and an optical detector collects returning light from the surface. Careful analysis of the returning light provides molecular information about the target samples including elemental composition, chemical bonds, and concentration.[12,13]

Since unique molecular fingerprints of organic compounds are present in the IR frequency region ranging from 30 to 300 THz (from 1 to 10 μm in wavelength), standoff detection based on IR spectroscopy is thought to be a promising technique for remote chemical detection and identification. One of the major challenges in developing state-of-the-art standoff IR spectroscopy is increasing sensitivity of the detector. Typical target analytes for the standoff detection such as explosives have low levels of traces on the surface due to their extremely low vapor pressure at room temperature. Vapor pressures of common explosives such as cyclotrimethylene trinitramine (RDX) and pentaerythritol tetranitrate (PETN) are on the order of 10^{-4} Pa (ref 14). The IR intensity is also significantly attenuated depending to the source-to-detector distance. In order to enhance the sensitivity, various types of uncooled IR sensors other than optical detectors have been proposed. Examples include mechanical transducers such as microstrings[15] and microcantilevers.[16] Yamada et al. reported the identification of airborne chemicals coated on the microstring resonator with picogram levels by monitoring the resonance frequency shift of the microstring due to the heat generated by IR absorbed molecules.[15] While they showed a very high sensitivity, the technique requires direct chemical deposition on the resonator; thus, it is not well-suited for standoff detection. Van Neste et al. reported the standoff detection of explosives by measuring the deflection of microcantilever induced by IR.[13] Although the

Received: July 5, 2016
Accepted: September 6, 2016

DOI: 10.1021/acs.analchem.6b02540
Anal. Chem. XXXX, XXX, XXX−XXX

microcantilever deflection was proportional to the amount of heat generated by IR irradiation reflected from the explosive molecules, deflection measurements in general suffer from nonspecific drifts. Toward performance enhancement of mechanical detectors beyond optical counterparts, research efforts have been focused on the modification of the physical size and shape of common solid-state microfabrication materials so as to increase their IR responsivity by decreasing stiffness and increasing surface area.[17−19] Surprisingly, there has been little effort toward exploration of new structural materials for mechanical transducers that are inherently sensitive to IR and thus ideal for various operation modes in standoff spectroscopy.

Here we demonstrate a standoff IR spectroscopy technique based on all hydrogel microcantilevers, which exhibit exceptional thermal and IR responsivity. We experimentally show that the poly(ethylene glycol) diacrylate (PEG-DA) hydrogel microcantilevers,[20] fabricated by cost-effective replica molding along with photopolymerization, exhibit significant resonance frequency shifts in response to heat and IR irradiation. This high thermal sensitivity makes these cantilevers an excellent candidate detector for standoff mechanical resonance spectroscopy (SMRS). The potential of this technique for field applications is demonstrated by the standoff detection of trace materials, dimethyl methyl phosphonate (DMMP) used as a nerve gas simulant, and RDX and PETN, explosives often used in military and industrial purposes, with high sensitivity and selectivity in ambient conditions.

EXPERIMENTAL SECTION

Chemicals. The PEG-DA prepolymer solution is prepared by mixing PEG-DA solution having a molecular weight of 250 (Sigma-Aldrich, St. Louis, MO) and photoinitiator [phenylbis-(2,4,6-trimethylbenzoyl)phosphine oxide] at the weight ratio of 98:2. The photoresist, SU8-2015 (Microchem, Westborough, MA) and poly(dimethylsiloxane) (PDMS, Sylgard 184) (Dow Corning, Midland, MI) were used as received. The DMMP (Sigma-Aldrich, Saint Louis, MO) was also used as purchased. RDX and PETN (AccuStandard, New Haven, CT) samples were in a mixture of methanol and acetonitrile at the weight ratio of 1:1 with a standard concentration of 1 mg/mL. They were used after evaporation of the solvent.

Fabrication of PEG-DA Microcantilevers. Figure 1a illustrates the fabrication process of PEG-DA hydrogel microcantilevers using the PDMS beam/handle mold assembly. PEG-DA microcantilevers were fabricated by UV curing of the PEGDA prepolymer inside the PDMS beam mold. A photoresist, SU8-2015, was spin-coated on a 4 in. silicon wafer for 30 s (5000 rpm for 10 μm target thickness) and then soft-baked for 4 min at 105 °C. The soft-baked photoresist was exposed to a 365 nm UV source (i-line, 17 mW/cm^2) for 15 s, developed, and hard-baked to define the SU8 cantilever master mold. To make the PDMS cantilever replica mold, a PDMS prepolymer mixture was prepared by mixing PDMS and curing agent with a 10:1 weight ratio, pouring onto the SU8 cantilever mold, and curing on a hot plate at 100 °C for 60 min (process 2, Figure 1). To make the PDMS handle mold, commercial silicon cantilever bases (PPP-NCHR, Nanosensors) with cantilever beams broken were placed in a Petri dish and the prepared PDMS prepolymer mixture was poured and cured on a hot plate at 100 °C for 60 min (processes 3−4, Figure 1). Although photocured rectangular SU8 blocks can be used as a master mold to define the thick handle of PEG-DA

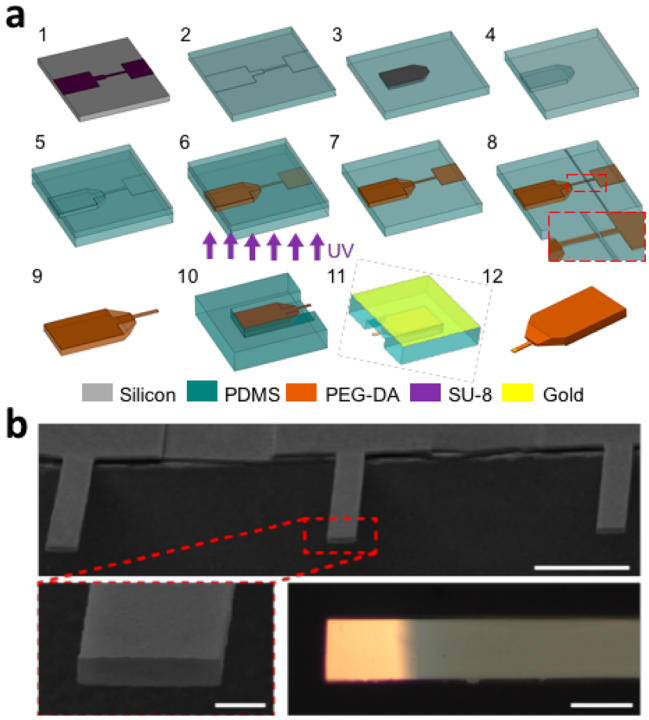

Figure 1. Fabrication process and scanning electron microscope (SEM) images of PEG-DA hydrogel microcantilevers. (a) 1, cantilever master mold; 2, cantilever mold PDMS replica; 3, PDMS handle mold with a silicon handle embedded; 4, cut the PDMS handle mold to have an inlet for hydrogel filling; 5, cut the PDMS cantilever mold; 6, align the PDMS handle mold with the PDMS cantilever mold, fill hydrogel, and cure with UV; 7, peel off the PDMS cantilever mold; 8, cut the cured PEG-DA with a desired length; 9, remove the PDMS handle mold; 10, place the PEG-DA microcantilever on the PDMS shadow mask; 11, deposit a thin metal (Ti/Au) film; 12, final device. (b) SEM images (top and bottom left) and optical image (bottom right) of the PEG-DA hydrogel microcantilever; 20/100 nm thick metal (Ti/Au) is coated at the free end of the microcantilever to enhance the light reflection for the optical measurement. Scale bars are 100, 10, and 50 μm for top, bottom left, and bottom right, respectively.

microcantilevers instead of the commercial silicon cantilever bases, the direct use of the commercial silicon bases can decrease the overall fabrication time and offer the better compatibility with commercial atomic force microscopy (AFM) cantilever holders.

The PDMS cantilever replica mold was aligned with the PDMS handle mold to make the cantilever/handle mold assembly. The PEG-DA prepolymer solution was prepared by mixing a PEG-DA solution (MW 250) and a photoinitiator [phenylbis(2,4,6-trimethylbenzoyl)phosphine oxide], then introduced into the aligned mold assembly. It was pipetted and introduced into the cantilever/handle mold assembly via capillary action and then cured with the UV light-emitting diode (LED) (CBT-90-UV-C31-M400-22, Luminus Devices, Sunnyvale, CA) for 5 s (UV dose: 590 mJ/cm^2) (processes 4−8, Figure 1). After the cantilever mold was separated from the handle mold, the cured PEG-DA microcantilever was cut to the desired length and detached from the handle mold (processes 8−9, Figure 1). While the width and thickness of PEG-DA microcantilevers are determined by the PDMS beam mold thus fixed to be 50 and 10 μm, respectively, various lengths can be easily offered. Because of variations in material properties (such as volume contraction or oxygen inhibition), the thickness of

DOI: 10.1021/acs.analchem.6b02540
Anal. Chem. XXXX, XXX, XXX−XXX

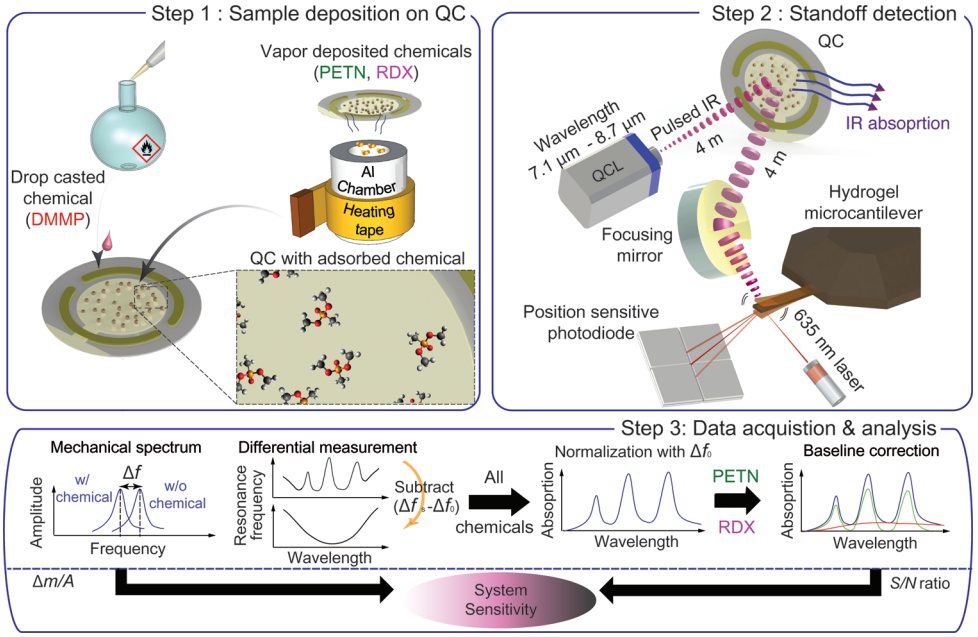

Figure 2. Summary schematic for the derivation of system sensitivity for each chemical: step 1, sample deposition on QC; step 2, standoff detection; step 3, data analysis. In the data analysis step, the adsorbed mass of chemical is measured by using the QC while the signal-to-noise (S/N) ratio for each chemical is derived from the standoff detection. To get the fractional frequency shift, the data obtained with a bare QC substrate (Δf_0) are subtracted from the data obtained with a target-coated QC substrate (Δf_s), then divided by Δf_0. Baselines in the fraction frequency shift spectra for vapor-deposited chemicals (RDX and PETN) are further corrected with multisegment linear lines.

the cantilevers varied between 10 and 10.2 μm. In order to enhance the reflectivity for optical measurement, 20/100 nm thick metal (Ti/Au) was subsequently deposited onto the top side of PEG-DA microcantilevers (processes 10−12, Figure 1).

Heating and IR Responses of PEG-DA Microcantilevers. While PEG-DA hydrogel microcantilevers were heated using the microceramic heater and GLTC-PX9 programmable temperature controller (Global Lab, Seoul, Korea) with the temperature resolution of 0.1 °C, resonance frequency shifts were measured. Prior to heating PEG-DA hydrogel microcantilevers, the microceramic heater temperature was calibrated using an indium-coated microcantilever by tracing its deflection curvature change at the crystallization and melting point of indium.[21] PEG-DA microcantilevers were directly mounted on the microceramic heater. The temperature was increased as a stepwise (5 °C interval and 2 min dwell at a specific temperature) from room temperature to 150 °C. The SR 760 spectrum analyzer (Stanford Research Systems, Sunnyvale, CA) was used to measure the resonance frequency of undriven PEG-DA microcantilevers by analyzing optical (635 nm) signals reflected from the PEG-DA microcantilever toward the position-sensitive diode (PSD) (SiTek Electro Optics, Partille, Sweden).

The UT-8 quantum cascade laser (QCL) (Daylight Solutions, San Diego, CA) was used as a wavelength tunable IR source. The QCL provides a tunable IR light from 7.1 to 8.7 μm with a spectral resolution of 5 nm. As a part of its operation, the QCL was pulsed at 200 kHz with a duty cycle of 10%. For the static mode measurement, the DS345 function generator (Stanford Research Systems, Sunnyvale, CA) was used to modulate the pulsed laser at 2 Hz. The PEG-DA and silicon microcantilevers were mounted on a stainless steel cantilever holder which was attached to the head unit of the multimode AFM (Bruker, Santa Barbara, CA). In order to measure the IR response of the microcantilevers, the QCL IR was directly irradiated on the microcantilevers and scanned from 7.1 to 8.7 μm. The SR760 spectrum analyzer and the SR 850 lock-in amplifier (Stanford Research Systems, Sunnyvale, CA) connected to the AFM head unit measured the resonance frequency in the dynamic mode and deflection in the static mode, respectively.

Standoff Spectroscopy. The standoff IR spectroscopy setup used in this study is shown in Figure 2. In order to estimate the sensitivity of our proposed detection system for DMMP, RDX, and PETN, we control the surface concentration of the three molecules adsorbed on the quartz crystal (QC). For the DMMP deposition, 10 μL of the DMMP solution was drop-cast using a pipet, thus evenly spread on a 1 in. diameter QC for uniform coating. The cast solution was kept at room temperature for 3−4 h until the bulk liquid of DMMP was evaporated and only a small amount of stain was left on the QC surface. This evaporation step prevents the diffraction of the IR laser on the surface of the bulk DMMP solution.

A vapor deposition method was used for RDX and PETN in order to evenly deposit them on the QC surfaces. A vapor generator, consisting of a heating platform, an aluminum cylindrical chamber that was wrapped with the heating tape (Omega, Stamford, CT), configured with a thermometer, and connected to a N_2 flow line (see Figure 2, step 1), was used in these experiments. A glass wool bundle was placed inside the aluminum chamber in order to increase the surface area for adsorption as well as accelerating the evaporation rates of RDX and PETN. Amounts of 100 μL of RDX and PETN solutions were added into the chamber using a syringe. The N_2 flow was kept at 200 sccm during the entire evaporation process, and temperature was kept at 90 °C for the first 15 min to evaporate the solvent of which boiling point is lower than 82 °C. After the removal of solvent, temperature was decreased and kept at 75 °C during the RDX and PETN evaporations. For RDX and

DOI: 10.1021/acs.analchem.6b02540
Anal. Chem. XXXX, XXX, XXX−XXX

PTEN depositions, the QC was placed 1 cm above the heating chamber.

Surface concentrations of the trace analytes on QCs were measured using the QCM-200 quartz crystal microbalance (Stanford Research Systems, Sunnyvale, CA). The change in mass (Δm) due to the adsorbed chemicals on the QC is obtained by using the Sauerbrey equation:[22]

$$\Delta f = \frac{2f_0^2}{A\sqrt{\rho_q \mu_q}}\Delta m \quad (1)$$

where f_0, A, ρ_q, and μ_q are the resonant frequency of unloaded crystal, active area of the crystal between the electrodes, density of quartz (2.65 g/cm^3), and shear modulus of quartz [2.95 × 10^{11} g/(cm·s^2)].

Next, we performed the standoff detection of each chemical by using the QCL and PEG-DA microcantilever (Figure 2, step 2). The IR beam emitted by the QCL was swept from wavelength of 7.2−8.4 μm. The QC with a target sample deposited was placed 4 m away from both the QCL and the PEG-DA microcantilever; thus, the total travel length of the IR from the QCL to the PEG-DA microcantilever became 8 m.

A focusing mirror was used in order to minimize the loss in IR power due to the scattering from the deposited materials on the QC surface. The resonance frequency of the PEG-DA microcantilever was measured using an AFM head unit as described above. Resonance frequency shifts of the PEG-DA microcantilevers were measured as a function of the IR wavelength with and without the target molecules deposition on the QC.

FT-IR Measurement. The IR spectra of DMMP, RDX, and PETN were characterized by using the Nicolet Continuum Fourier transform infrared spectroscopy (FT-IR) instrument (ThermoFisher Scientific, Bellefonte, PA). Samples were drop-cast onto the gold-coated silicon wafer and were left until the solvents of RDX and PETN solutions were evaporated. The FT-IR spectra were obtained in the reflection mode. The number of registered scans was 200 with resolution of 4 cm^{-1}.

RESULTS AND DISCUSSION

Figure 3a shows the resonance frequencies of the 12 PEG-DA microcantilevers with various lengths ranging from 245 and 400 μm. The inset shows the amplitude spectrum around the fundamental resonance frequency and its Lorentzian fit for a 300 μm long PEG-DA microcantilever. The resonance frequency measurement without any external drive was performed for each PEG-DA microcantilever at room temperature, and the data were collected using the spectrum analyzer. The resonance frequency decreases from 42.5 to 14.2 kHz as the beam length increases from 245 to 400 μm. Measurements are in good agreement with the theoretical relationship between resonance frequency and beam length is given by the following equation:[23]

$$f_1 = \frac{\lambda_1^2}{2\pi\sqrt{12}}\frac{t}{l^2}\sqrt{\frac{E}{\rho}} \quad (2)$$

where f_1 and λ_1 are the first mode resonance frequency and eigenvalue of the microcantilever beam. t, l, E, and ρ are the thickness, length, Young's modulus, and mass density of the microcantilever beam, respectively. For aforementioned theoretical estimates, Young's modulus of 1.42 ± 0.1 GPa from ref 20 was used for all PEG-DA microcantilevers since they were made out of the same material, PEG-DA MW 250, and under the same UV dose for a single batch. The same Young's modulus was also used to calculate spring constant of PEG-DA microcantilevers by

$$k = \frac{Ewt^3}{4l^3} \quad (3)$$

where w is the width of the microcantilever. Calculated spring constants are 1.2 and 0.3 N/m for 245 and 400 μm long PEG-DA microcantilevers, respectively. While the width and thickness of PEG-DA microcantilevers are fixed due to the beam mold geometry, the spring constant as well as the length can be easily tuned by the precision cutting after curing.[20]

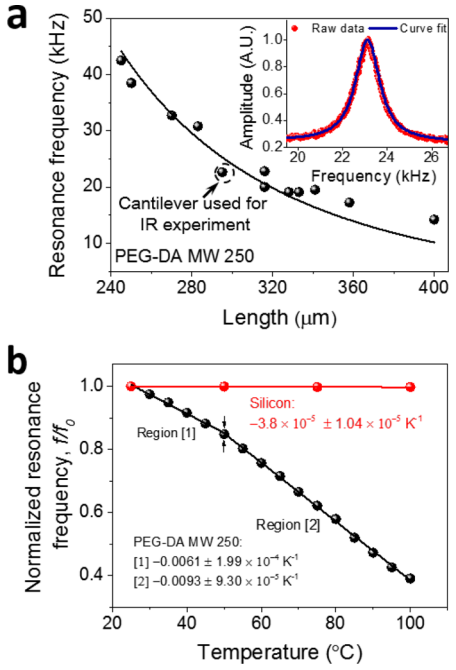

Figure 3. (a) Fundamental resonance frequencies of the 12 PEG-DA MW 250 microcantilevers (thickness, 10 μm; width, 50 μm) as a function of the beam length. The fitting lines accord to the inverse proportion to the square of the beam length. The inset shows the resonance frequency response of a 300 μm long PEG-DA microcantilever and its Lorentzian fit. (b) Normalized resonance frequencies of the PEG-DA and silicon microcantilevers as a function of heating temperature. Data for the silicon microcantilever are adopted from ref 24. The slope of linear fitting lines for the PEG-DA microcantilever changes at around 50 °C.

Figure 3b shows the normalized resonance frequency of the 300 μm long PEG-DA microcantilever as a function of temperature while the microcantilever is heated on the microceramic heater. The normalized resonance frequency change of a silicon microcantilever upon heating[24] is also included for comparison. The PEG-DA microcantilever exhibits larger decrease in the resonance frequency upon heating compared to the silicon microcantilever. With an increase of temperature from 25 to 100 °C, the fundamental resonance frequency (first flexural mode) of the PEG-DA microcantilever decreases from 22.8 to 8.9 kHz, exhibiting about 60% shift. The thermal sensitivity of the PEG-DA microcantilever, the slope in the normalized resonance frequency versus temperature plot, is −0.0061/K for room temperature to 50 °C (region 1 in Figure 3b) and −0.0093/K for 50−100 °C (region 2 in Figure 3b), respectively. The transition of the slope at 50 °C seems to be a

DOI: 10.1021/acs.analchem.6b02540
Anal. Chem. XXXX, XXX, XXX−XXX

transition to a rubbery state of polymers beyond which their Young's moduli sharply decrease with heating. The thermal sensitivities of the PEG-DA microcantilever in these two temperature ranges are 2 orders of magnitude higher than that of the silicon microcantilever used for comparison. Such huge decrease in the resonance frequency of the PEG-DA microcantilever upon heating is mainly attributed to the decrease in its Young's modulus since the effect of thermal expansion of the PEG-DA microcantilever on the resonance frequency change is less than 5% upon heating from room temperature to 100 °C based on the thermal expansion coefficient of ~600 ppm/K for PEG with similar molecular weight (MW 400) found in literatures.[25−28] Upon further heating, the resonance frequency of the PEG-DA microcantilever keeps decreasing until ~120 °C, and then it becomes insensitive to heating (see Supporting Information Figure S1). Therefore, the temperature of ~120 °C is thought to be another phase transition of the PEG-DA MW 250. Figure S1 also shows the negligible effect of the thermal expansion on the resonance frequency upon heating. Unless the effect of the thermal expansion is weak, the normalized resonance frequency plots cannot be collapsed on top of each other.

The IR response of 300 μm long PEG-DA microcantilever for both dynamic and static modes is obtained by scanning the IR wavelength from 7.1 to 8.7 μm (with the wavelength increment of 5 nm) as shown in Figure 4a. The optical power of the QCL can be controlled by adjusting the current from 800 to 1100 mA by using a separate controller. Under the IR laser illumination, the resonance frequency of the PEG-DA microcantilever noticeably drops due to its large IR absorption and high thermal sensitivity.

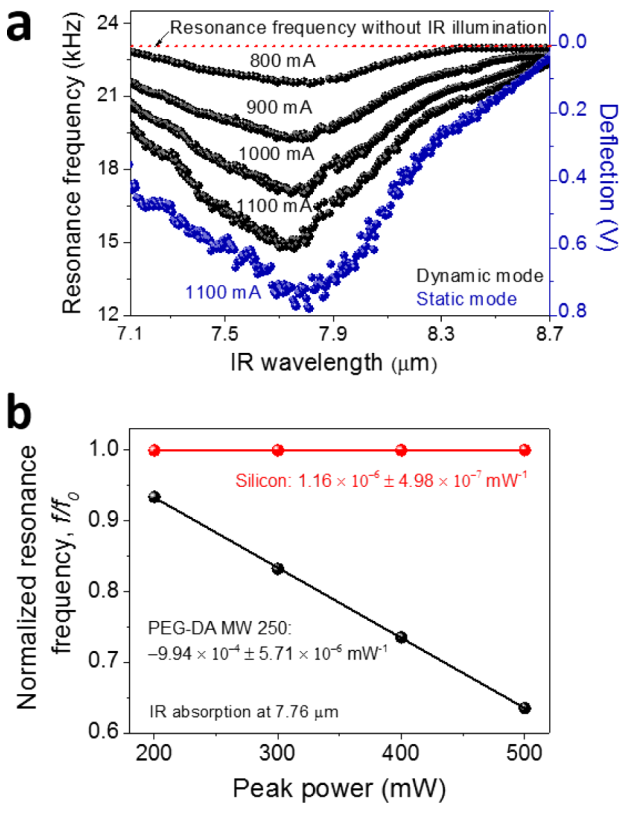

Figure 4. (a) Resonance frequency variations of the PEG-DA microcantilever responding to the pulsed IR illumination with different QCL currents. The wavelength of IR is scanned from 7.1 to 8.7 μm. Deflection of the PEG-DA microcantilever in a static mode (dark blue) is included for comparison. (b) Normalized resonance frequency changes of the PEG-DA and silicon microcantilevers as a function of the incident IR power. Straight lines are linear fits of measured data points.

There resonance frequency shift (dynamic mode) and the change in deflection (static mode) of the PEG-DA microcantilever upon IR illumination show similar trends as shown in Figure 4a. The IR light is pulsed at a rate of 2 Hz in order to fully excite and relax the cantilever since the PEG-DA microcantilever has a high thermal inertia and, therefore, a larger time constant (see Supporting Information Figure S2). The noise level in the dynamic mode is more suppressed than that in the static mode where the deflection of the PEG-DA microcantilever is measured in time domain. The shapes of IR spectra in both modes are convex downward due to the power variation of the IR in that region. The IR power increases as the wavelength increases from 7.1 to 7.8 μm and then decreases as the wavelength increases from 7.8 to 8.7 μm (see Supporting Information Figure S3).

Figure 4b presents a comparison of the magnitude of resonance frequency drop for the PEG-DA and silicon microcantilevers as a function of the incident IR peak power for the IR wavelength fixed at 7.76 μm. They have similar resonance frequencies in ambient conditions (22.8 and 21.3 kHz for PEG-DA and silicon microcantilevers, respectively) but significantly different resonance frequency variations upon IR irradiation. The resonance frequency of the PEG-DA microcantilever remarkably decreases, whereas the resonance frequency shift for the silicon microcantilever is negligible. This confirms that the PEG-DA microcantilever exhibits a higher IR sensitivity than the silicon microcantilever for the dynamic mode of operation. The straight lines are linear fits of measured data points showing that the decrease of the resonance frequency is proportional to the incident IR peak power. It should be noted that the extrapolation of the PEG-DA linear fitting line does not cross original value (f_0) at the zero IR peak power. This might be because the incident IR was absorbed by other components such as water and organic molecules adsorbed on the surface of PEG-DA microcantilever from the ambient air. It can cause a nonlinearity between the resonance frequency shift and peak power for the lower power range of IR.

Parts a and b of Figure 5 show the chemical structures of target chemicals (DMMP, RDX, and PETN) and the standoff IR spectra of trace target molecules measured with the PEG-DA microcantilever detector at 4 m away from each target. The wavelength of the IR was scanned (with 200 kHz repetition rate and 10% duty cycle) from 7.2 to 8.4 μm. A fractional method is employed in order to remove the effects of the IR peak power variation and the IR absorptivity variation of the PEG-DA for the IR wavelength. In the fractional method, the standoff IR spectrum, $s(\Delta f)$, can be formulated by

$$s(\Delta f) = \frac{\Delta f_s - \Delta f_0}{\Delta f_0} \quad (4)$$

where Δf_s and Δf_0 are the resonance frequency shifts of the PEG-DA microcantilever by IR irradiation reflected from the sample deposited and the bare QC surfaces, respectively. Δf_s and Δf_0 are measured while the wavelength of the QCL IR is scanned from 7.2 to 8.4 μm. Then, the subtracted signal ($\Delta f_s - \Delta f_0$) is normalized with respect to Δf_0. A detailed data

DOI: 10.1021/acs.analchem.6b02540
Anal. Chem. XXXX, XXX, XXX−XXX

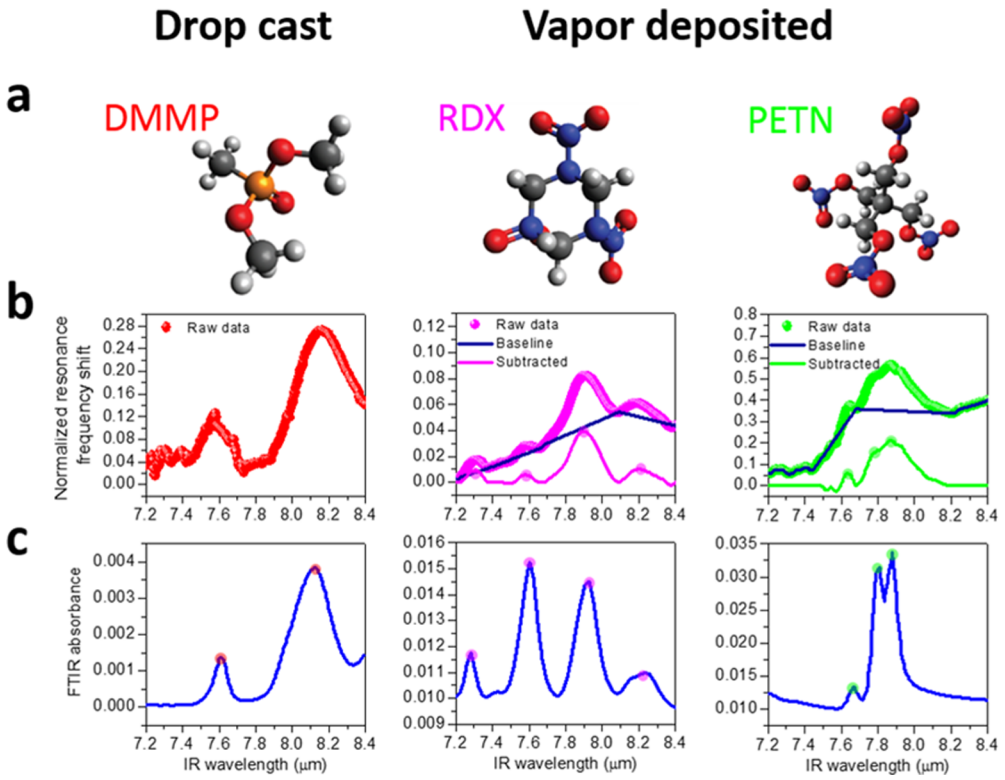

Figure 5. (a) Chemical structures of the standoff target molecules (orange, phosphorus; black, carbon; gray, hydrogen; red, oxygen; blue, nitrogen). (b) Standoff IR spectra of DMMP, RDX, and PETN using the PEG-DA microcantilever (MW 250) for the distance of 4 m. Surface densities of the adsorbed molecules on QCs are measured to be 2.14, 9.09, and 2.05 $\mu g/cm^2$ for DMMP, RDX, and PETN, respectively. (c) FT-IR spectra of the target molecules as references for the SMRS spectra.

processing method is described in the Supporting Information (see Figure S4).

When the frequency of the illuminating IR light matches the molecular vibration frequency, resonant absorption takes place, and a plot of transmitted/reflected IR intensity as a function of wavelength shows IR absorption peaks. For DMMP, absorption peaks appear at 7.60 and 8.14 μm. These peaks are attributed to deformation of CH_3P and P═O stretching, respectively.[29,30] For RDX, peaks that appear at 7.27, 7.55, and 7.88 μm are due to symmetric vibration from the nitro groups bound to nitrogen ($N-NO_2$), while the peak at 8.11 μm originates from stretching of N−C−N ring.[31] In the case of PETN, peaks that appear at 7.65, 7.80, and 7.90 μm are due to stretch vibrations of the nitro groups bound to oxygen ($O-NO_2$).[16] All these observations with PEG-DA microcantilevers are in good agreement with the corresponding FT-IR absorption spectra as shown in Figure 5c.

While the spectrum for DMMP shows a flat baseline, the spectra for RDX and PETN exhibit baseline drifts which we believe are nonspecific to the sample (see raw data in Figure 5b). These are possibly due to the difference in the sample preparation methods. For the DMMP drop-casting method, the position and angle of QC were not changed during the sample deposition. The position and angle of the reflected IR from the QC surface also remained unchanged during the entire standoff measurements. On the other hand, RDX and PETN samples were deposited on the QC surface by the vapor deposition method. Once Δf_0 was measured from the bare QC, it was taken out and placed above the vapor generator (aluminum heating chamber) to deposit the samples, and then brought back to the original position for the standoff measurement. This causes an inevitable variation in the alignment of the IR laser, which possibly generates offsets or drifts in the spectrum baseline. Due to this reason, an additional data processing, a multisegment linear baseline correction,[32] is necessary for RDX and PETN as shown in Figure 5b. In addition, the peak-to-peak ratios from SMRS are not well-matched with those from the reference benchtop FT-IR. This is possibly because of two different working principles of FT-IR and SMRS. The former technique follows the Beer−Lambert law to measure IR absorption, while SMRS is based on nonradiative decay, which is complementary to the Beer−Lambert law. Due to the two different mechanisms involved in detection, the observed peak intensities are different as shown in Figure 5.

The surface concentrations of DMMP, RDX, and PETN on QC were 2.14, 9.09, and 2.05 $\mu g/cm^2$, respectively. It is assumed that the IR absorbance from the molecules on the surface is proportional to the concentration of the molecules on the QC.[33] In order to estimate the maximum performance of our standoff system using the PEG-DA microcantilever, the limits of detection (LODs) of the three target samples were calculated from the highest IR peak intensities in the spectra and surface concentrations of the target traces on the QC. The LODs were determined by comparing the signal-to-noise ratio (S/N) of 3 to the height of the main IR characterization peaks for the measured concentrations. The calculated LODs were approximately 80 ng/cm^2 for DMMP at 8.14 μm, 600 ng/cm^2 for RDX at 7.88 μm, and 40 ng/cm^2 for PETN at 8.14 μm, respectively.

To our knowledge, this is the first successful demonstration of PEG-DA hydrogel microcantilever application in standoff IR spectroscopy. After demonstrating the high thermal sensitivity of PEG-DA microcantilevers in the dynamic mode due to

DOI: 10.1021/acs.analchem.6b02540
Anal. Chem. XXXX, XXX, XXX−XXX

heating and IR irradiation, selective detection of three different chemicals was performed with comparable LOD values reported recently[10,11] without any optimization in terms of the geometry, shape, and material composition of the device. It is evident that there would be more room for performance improvement by employing hydrogels with different molecular weights and functional groups and further optimization of device geometries.

CONCLUSION

We have successfully developed a standoff detection system for surface adsorbed chemicals by using IR-sensitive PEG-DA microcantilevers. The hydrogel microcantilevers with high sensitivity to IR-induced heating were prepared through UV curing of PEG-DA introduced into the PDMS mold assembly. The resonance frequency of the PEG-DA microcantilevers varies significantly under IR absorption because the changes in the Young's modulus of the PEG-DA. Using PEG-DA microcantilevers, standoff detection of DMMP, RDX, and PETN with high sensitivity and selectivity was demonstrated for the target chemicals placed at a distance of 4 m. In the case of PETN, the demonstrated LOD was 40 ng/cm^2. Overall, implementation of the PEG-DA hydrogel microcantilevers as mechanical transducers to enhance the sensitivity in the standoff IR spectroscopy appears to be very promising since hydrogel microcantilevers offer higher temperature-dependent material property variation as well as small physical dimension, low power consumption, and no requirement of cooling.

ASSOCIATED CONTENT

Supporting Information

The Supporting Information is available free of charge on the ACS Publications website at DOI: 10.1021/acs.analchem.6b02540.

Thermal response and static mode response to IR of PEG-DA microcantilevers, peak power curve of UT-8 QCL, and signal processing method of standoff spectrum (PDF)

AUTHOR INFORMATION

Corresponding Authors

*E-mail: jayclee@sogang.ac.kr.
*E-mail: thundat@ualberta.ca.

Notes

The authors declare no competing financial interest.

ACKNOWLEDGMENTS

This work was supported by the Canada Excellence Research Chairs (CERC) program, the Commercializations Promotion Agency for R&D Outcomes (COMPA) (2015K000127), and the National Research Foundation of Korea (NRF) funded by the Korea government (MSIP) (NRF-2013R1A1A1076080, NRF-2014R1A2A1A11053283, and NRF-2016R1A2B3014157). The authors thank Mr. Jaeseol Lee for his assistance regarding device fabrication used in the early stage of this work.

REFERENCES

(1) Hemmer, P. R.; Miles, R. B.; Polynkin, P.; Siebert, T.; Sokolov, A. V.; Sprangle, P.; Scully, M. O. *Proc. Natl. Acad. Sci. U. S. A.* **2011**, *108*, 3130−3134.
(2) Morales-Rodríguez, M. E.; Van Neste, C. W.; Senesac, L. R.; Mahajan, S. M.; Thundat, T. *Sens. Actuators, B* **2012**, *161*, 961−966.
(3) Katz, O.; Natan, A.; Silberberg, Y.; Rosenwaks, S. *Appl. Phys. Lett.* **2008**, *92*, 171116.
(4) López-Moreno, C.; Palanco, S.; Javier Laserna, J.; DeLucia, F., Jr.; Miziolek, A. W.; Rose, J.; Walters, R. A.; Whitehouse, A. I. *J. Anal. At. Spectrom.* **2006**, *21*, 55−60.
(5) Gaft, M.; Nagli, L. *Opt. Mater. (Amsterdam, Neth.)* **2008**, *30*, 1739−1746.
(6) Gottfried, J. L.; De Lucia, F. C.; Munson, C. A.; Miziolek, A. W. *Appl. Spectrosc.* **2008**, *62*, 353−363.
(7) Ali, E. M. A.; Edwards, H. G. M.; Scowen, I. J. *J. Raman Spectrosc.* **2009**, *40*, 2009−2014.
(8) Sharma, S. K.; Lucey, P. G.; Ghosh, M.; Hubble, H. W.; Horton, K. A. *Spectrochim. Acta, Part A* **2003**, *59*, 2391−2407.
(9) Gottfried, J. L.; De Lucia, F. C.; Munson, C. a.; Miziolek, A. W. *Spectrochim. Acta, Part B* **2007**, *62*, 1405−1411.
(10) Van Neste, C. W.; Senesac, L. R.; Yi, D.; Thundat, T. *Appl. Phys. Lett.* **2008**, *92*, 134102.
(11) Liu, X.; Van Neste, C. W.; Gupta, M.; Tsui, Y. Y.; Kim, S.; Thundat, T. *Sens. Actuators, B* **2014**, *191*, 450−456.
(12) Wallin, S.; Pettersson, A.; Östmark, H.; Hobro, A. *Anal. Bioanal. Chem.* **2009**, *395*, 259−274.
(13) Van Neste, C. W.; Senesac, L. R.; Thundat, T. *Anal. Chem.* **2009**, *81*, 1952−1956.
(14) Pushkarsky, M. B.; Dunayevskiy, I. G.; Prasanna, M.; Tsekoun, A. G.; Go, R.; Patel, C. K. N. *Proc. Natl. Acad. Sci. U. S. A.* **2006**, *103*, 19630−19634.
(15) Yamada, S.; Schmid, S.; Larsen, T.; Hansen, O.; Boisen, A. *Anal. Chem.* **2013**, *85*, 10531−10535.
(16) Krause, A. R.; Van Neste, C.; Senesac, L.; Thundat, T.; Finot, E. *J. Appl. Phys.* **2008**, *103*, 094906.
(17) Chae, I.; Lee, D.; Kim, S.; Thundat, T. *Anal. Chem.* **2015**, *87*, 7125−7132.
(18) Greeneltch, N. G.; Blaber, M. G.; Henry, A.-I.; Schatz, G. C.; Van Duyne, R. P. *Anal. Chem.* **2013**, *85*, 2297−2303.
(19) Brown, L. V.; Yang, X.; Zhao, K.; Zheng, B. Y.; Nordlander, P.; Halas, N. J. *Nano Lett.* **2015**, *15*, 1272−1280.
(20) Lee, J. S.; Song, J.; Kim, S. O.; Kim, S.; Lee, W.; Jackman, J. A.; Kim, D.; Cho, N.-J.; Lee, J. *Nat. Commun.* **2016**, *7*, 11566.
(21) Yim, C.; Yun, M.; Kim, S.; Jung, N.; Lim, S.-H.; Lee, M.; Rhee, S.-W.; Thundat, T.; Jeon, S. *Jpn. J. Appl. Phys.* **2012**, *51*, 08KB07.
(22) Lee, D.; Yoo, M.; Seo, H.; Tak, Y.; Kim, W.-G.; Yong, K.; Rhee, S.-W.; Jeon, S. *Sens. Actuators, B* **2009**, *135*, 444−448.
(23) Yi, J. W.; Shih, W. Y.; Shih, W.-H. *J. Appl. Phys.* **2002**, *91*, 1680.
(24) Lee, J.; Goericke, F.; King, W. P. *Sens. Actuators, A* **2008**, *145*−*146*, 37−43.
(25) Gautam, P. K.; Saroj, R. S.; Gautam, R. K.; Pandey, J. D. *Natl. Acad. Sci. Lett.* **2015**, *38*, 153−156.
(26) Tsujita, Y.; Nose, T.; Hata, T. *Polym. J.* **1973**, *5*, 201−207.
(27) Mertens, J.; Finot, E.; Thundat, T.; Fabre, A.; Nadal, M.-H.; Eyraud, V.; Bourillot, E. *Ultramicroscopy* **2003**, *97*, 119−126.
(28) Rúa, A.; Fernández, F. E.; Hines, M. A.; Sepúlveda, N. *J. Appl. Phys.* **2010**, *107*, 053528.
(29) Brunol, E.; Berger, F.; Fromm, M.; Planade, R. *Sens. Actuators, B* **2006**, *120*, 35−41.
(30) Bowen, J. M.; Powers, C. R.; Ratcliffe, A. E.; Rockley, M. G.; Hounslow, A. W. *Environ. Sci. Technol.* **1988**, *22*, 1178−1181.
(31) Infante-Castillo, R.; Pacheco-Londoño, L.; Hernández-Rivera, S. P. *Spectrochim. Acta, Part A* **2010**, *76*, 137−141.
(32) Krafft, C.; Kirsch, M.; Beleites, C.; Schackert, G.; Salzer, R. *Anal. Bioanal. Chem.* **2007**, *389*, 1133−1142.
(33) Kim, S.; Lee, D.; Liu, X.; Van Neste, C.; Jeon, S.; Thundat, T. *Sci. Rep.* **2013**, *3*, 1111.

DOI: 10.1021/acs.analchem.6b02540
Anal. Chem. XXXX, XXX, XXX−XXX